BIOCHEMISTRY
including biophysical chemistry & molecular biology

Article

pubs.acs.org/biochemistry

Distinct Substrate Selectivity of a Metabolic Hydrolase from *Mycobacterium tuberculosis*

Jessica K. Lukowski,[†,§] Christopher P. Savas,[†,§] Alexandra M. Gehring,[†] Magy G. McKary,[†] Chinessa T. Adkins,[‡] Luke D. Lavis,[‡] Geoffrey C. Hoops,[†] and R. Jeremy Johnson*[,†]

[†]Department of Chemistry, Butler University, 4600 Sunset Avenue, Indianapolis, Indiana 46208, United States

[‡]Janelia Research Campus, The Howard Hughes Medical Institute, 19700 Helix Drive, Ashburn, Virginia 20147, United States

Supporting Information

ABSTRACT: The transition between dormant and active *Mycobacterium tuberculosis* infection requires reorganization of its lipid metabolism and activation of a battery of serine hydrolase enzymes. Among these serine hydrolases, Rv0045c is a mycobacterial-specific serine hydrolase with limited sequence homology outside mycobacteria but structural homology to divergent bacterial hydrolase families. Herein, we determined the global substrate specificity of Rv0045c against a library of fluorogenic hydrolase substrates, constructed a combined experimental and computational model for its binding pocket, and performed comprehensive substitutional analysis to develop a structural map of its binding pocket. Rv0045c showed strong substrate selectivity toward short, straight chain alkyl esters with the highest activity toward four atom chains. This strong substrate preference was maintained through the combined action of residues in a flexible loop connecting the cap and α/β hydrolase domains and in residues close to the catalytic triad. Two residues bracketing the substrate-binding pocket (Gly90 and His187) were essential to maintaining the narrow substrate selectivity of Rv0045c toward various acyl ester substituents, as independent conversion of these residues significantly increased its catalytic activity and broadened its substrate specificity. Focused saturation mutagenesis of position 187 implicated this residue, as the differentiation point between the substrate specificity of Rv0045c and the structurally homologous ybfF hydrolase family. Insertion of the analogous tyrosine residue from ybfF hydrolases into Rv0045c increased the catalytic activity of Rv0045 by over 20-fold toward diverse ester substrates. The unique binding pocket structure and selectivity of Rv0045c provide molecular indications of its biological role and evidence for expanded substrate diversity in serine hydrolases from *M. tuberculosis*.

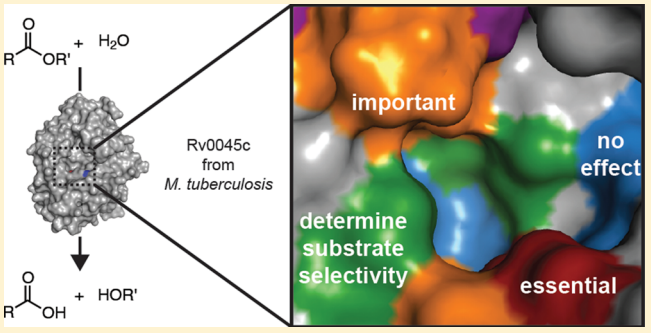

The transition between dormant and active *Mycobacterium tuberculosis* infection requires the reorganization of its cellular and lipid metabolism.[1−3] The importance of lipid metabolism to the survival of *M. tuberculosis* is highlighted by the presence of over 250 *M. tuberculosis* genes annotated as involved in lipid metabolism, whereas bacteria such as *Escherichia coli* have only 50 genes proposed to be involved in lipid metabolism.[4] Among the genes required for lipid metabolism in *M. tuberculosis* are over 30 genes predicted to encode serine hydrolases due to the presence of a conserved G-X-S-X-G motif and a proposed α/β hydrolase fold.[5] The importance of serine hydrolases to metabolism and dormant infection in *M. tuberculosis* has already made them exciting targets for inhibition and therapeutic design.[6,7] The expansion of serine hydrolase activity in *M. tuberculosis* also suggests unique environmental niches and likely divergent substrate specificities among mycobacterial serine hydrolases.[4,5,8] With the ongoing exploitation of serine hydrolases as novel biocatalysts, the serine hydrolases from *M. tuberculosis* represent an unexplored but potentially rich source of hydrolase scaffolds for protein engineering.[9,10] Characterization of the *in vitro* substrate specificity of nine mycobacterial serine hydrolases showcased the broad reactivity present within this enzyme family, which includes measurable enzymatic activity toward straight chain esters, vinyl esters, and triacylglycerols (TAGs).[6]

Among mycobacterial hydrolases, Rv0045c from *M. tuberculosis* has limited sequence similarity to other bacterial hydrolases and showed only weak substrate selectivity toward straight-chain *p*-nitrophenyl esters, making predictions of its biological activity and physiological importance difficult.[11−13] The three-dimensional structure of Rv0045c and its structural alignment showed that Rv0045c was, however, structurally similar to two different families of serine hydrolases: the ybfF hydrolase from *Escherichia coli* and the (*E*)-2-(acetamidomethylene) succinate (*E*-2AMS) hydrolase from *Mesorhizobium loti*.[13−15] These two families of bacterial hydrolases, however, catalyze distinct metabolic reactions, complicating the prediction of the natural reactivity and substrate specificity for

Received: September 2, 2014
Revised: October 29, 2014
Published: October 29, 2014

dx.doi.org/10.1021/bi501108u | *Biochemistry* 2014, 53, 7386−7395

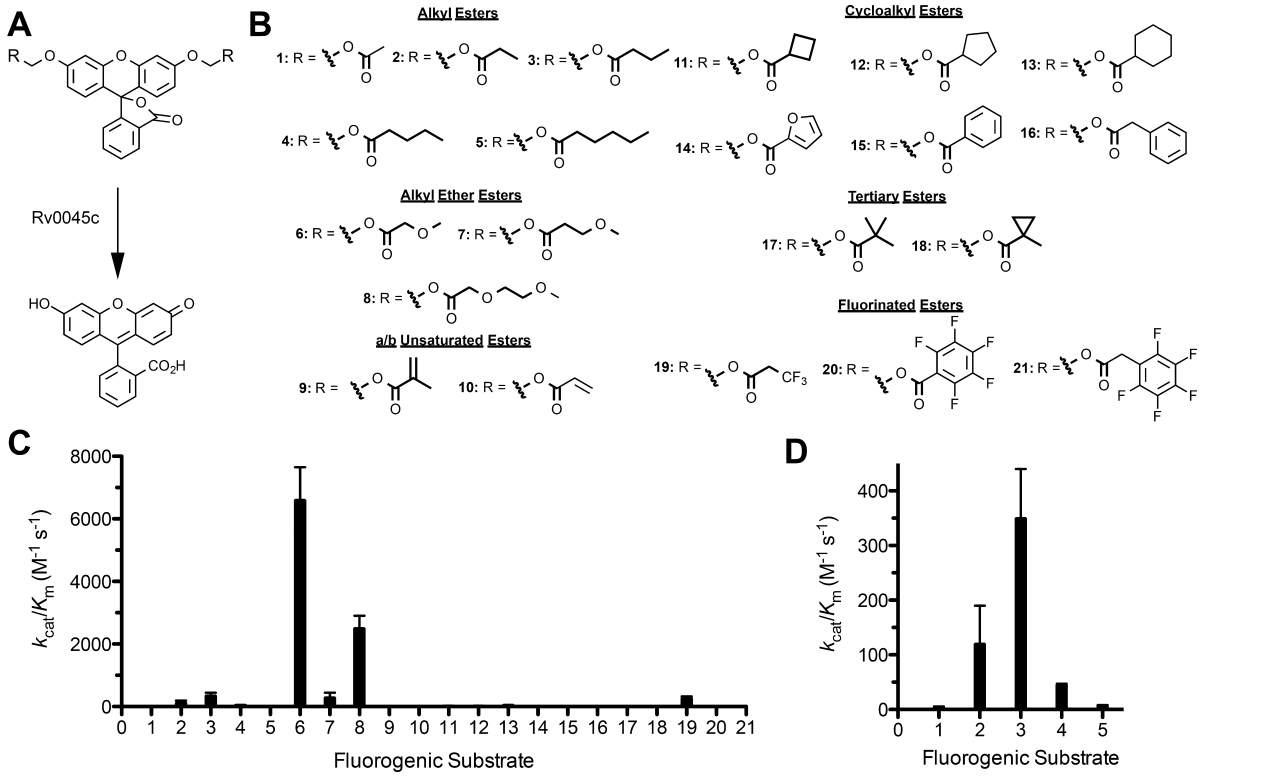

Figure 1. Substrate specificity of Rv0045c against fluorogenic hydrolase substrates. (A) Activation of the fluorogenic substrates by Rv0045c. Hydrolysis of the ester bond on the diacyloxymethyl ether fluorescein substrates by Rv0045c converts the fluorescein core from the nonfluorescent lactone form to the highly fluorescent quinoid form. The rate of fluorophore activation is measured at a range of substrate concentrations to determine the kinetic constants for fluorophore activation. (B) Fluorogenic substrate library. Each of the substrates is composed of diacyloxymethyl ether fluorescein (1A) with varying R-groups. The differing R-groups have been organized into classes based on chemical functionality. All of the substrates were synthesized as described previously.[18,22,39] (C) Global comparison of the catalytic specificity (k_{cat}/K_M) of Rv0045c against each of the 21 substrates (structures and numbering given in panel B). (D) Substrate specificity of Rv0045c against alkyl ester substrates, illustrating the substrate selectivity based on the carbon chain length. Detailed kinetic results for each substrate are provided in Supplemental Table 1, Supporting Information.

Rv0045c.[16−18] The ybfF hydrolases are proposed to catalyze the hydrolysis of thioesters in malonyl- or succinyl-CoA but are also capable of interesting biocatalysis reactions using their bifurcated binding pocket.[14,16−18] In comparison, *E*-2AMS hydrolases catalyze the unusual and complicated final step in the bacterial degradation of vitamin B_6 to succinic semialdehyde, ammonia, acetate, and carbon dioxide.[15] Each of these three hydrolase families contains a two helical structural cap that controls their divergent substrate specificity, as the loop connecting the cap domain to the α/β hydrolase domain forms the binding pocket of the ybfF and *E*-2AMS hydrolases.[13,15,18] Electron density for this loop was unfortunately absent in the final structure of Rv0045c, and so the importance of this key structural loop to controlling the substrate specificity of Rv0045c is unknown.[13]

Herein, we characterize the chemical reactivity of Rv0045c from *M. tuberculosis*, determine the global substrate specificity of Rv0045c using a library of fluorogenic hydrolase substrates, and map the structural features controlling this substrate specificity using a combination of comprehensive alanine-scanning mutagenesis, kinetic analysis, and computer modeling. Key structural features controlling the substrate specificity of Rv0045c are identified that bracket the binding pocket and that differentiate the substrate specificity of Rv0045c from structurally similar bacterial hydrolases. Substitution analysis based on homologous hydrolases also identifies variants of Rv0045c with significantly increased catalytic activity against a range of ester substrates, providing potential lead variants for biocatalyst design. The unique sequence and structural composition of Rv0045c and the expansion of hydrolase scaffolds in *M. tuberculosis* make Rv0045c an interesting biocatalyst target. Our comprehensive substrate specificity and structural map of Rv0045c provide molecular indications of the biological role of Rv0045c and evidence for the expanded substrate diversity in serine hydrolases from *M. tuberculosis*.

EXPERIMENTAL PROCEDURES

Overexpression and Purification of Rv0045c Protein. Rv0045c protein was overexpressed in *E. coli* as an N-terminal 6xHis-tag fusion using a bacterial expression plasmid (pET28a) containing the Rv0045c gene from *M. tuberculosis* as previously described.[12,13] This bacterial plasmid (pET28-Rv0045c) was transformed into *E. coli* BL21 (DE3) RIPL cells (Agilent, La Jolla, CA). A saturated overnight culture of *E. coli* BL21 (DE3) RIPL (pET28-Rv0045c) in LB media containing kanamycin (40 μg/mL) and chloramphenicol (30 μg/mL) was used to inoculate LB-media (250 mL) containing kanamycin (40 μg/mL) and chloramphenicol (30 μg/mL), and the bacterial culture was grown with constant shaking (225 rpm) at 37 °C. When the OD_{600} reached 0.6−0.8, the temperature of the culture was decreased to 16 °C and isopropyl β-D-1-thiogalactopyranoside (IPTG) was added to a final concentration of 1.0 mM. Protein induction proceeded overnight

dx.doi.org/10.1021/bi501108u | *Biochemistry* 2014, 53, 7386−7395

(~16–20 h) at 16 °C. Bacterial cultures were collected by centrifugation at 6000*g* for 10 min at 4 °C. The bacterial cell pellet was resuspended in PBS (5 mL) and stored at −20 °C. To disrupt the bacterial cell wall, lysozyme (50 mg; Sigma-Aldrich) and 10× Bug Buster solution (700 μL; EMD Millipore) were added to the thawed cell pellet; cell lysis proceeded on an orbital shaker for 1 h at 4 °C. To remove insoluble cell material, lysed cells were centrifuged at 16000*g* for 10 min at 4 °C. Ni-NTA agarose (600 μL; Qiagen, Valencia, CA) was added to the soluble fraction and allowed to incubate at 4 °C for 30–60 min. The resin was washed three times with PBS containing increasing concentrations of ice-cold imidazole (30 mL each of PBS containing 10 mM imidazole, 25 mM imidazole, or 50 mM imidazole) and recollected by centrifugation at 2000*g* for 2 min at 4 °C. Rv0045c was eluted in PBS containing 250 mM imidazole (1.0 mL) and dialyzed (10K MWCO; Pierce, Rockford, IL) against PBS overnight at 4 °C with constant stirring.

The purity of Rv0045c was confirmed by SDS–PAGE on a 4–20% gradient gel (Novex-LifeTechnologies) visualized with colloidal Coomassie brilliant blue; the purity was shown to be greater than 95% (Supplemental Figure 2, Supporting Information). The concentration of Rv0045c was determined by measuring the absorbance at 280 nm and converted to molarity units with an extinction coefficient of ε^{280} = 35 980 M^{-1} cm^{-1} calculated from the theoretical amino acid sequence using the ProtParam online proteomics tool on the ExPASy Web site (http://web.expasy.org/protparam).[19]

Site-Directed Mutagenesis and Purification. Variants of Rv0045c were produced by QuikChange II site-directed mutagenesis of pET28-Rv0045c template DNA using a derivation of the manufacturer's suggested procedure (Agilent, Santa Clara, CA), the only exception being specific annealing temperatures and the mutagenesis primers (Integrated DNA Technologies, Coralville, IA) outlined in Supplementary Table 6, Supporting Information. Mutagenic PCR products were subjected to digestion with DpnI restriction endonuclease for 1 h at 37 °C to degrade wild-type template plasmid DNA. Mutated pET28-Rv0045c plasmid DNA was replicated by transformation into *E. coli* DH5α cells, followed by plasmid DNA isolation/purification from saturated overnight cultures using a commercial kit (IBI Scientific, Peosta IA). Proper mutations in the Rv0045c DNA sequence were confirmed by DNA sequencing (Genewiz, South Plainfield, NJ) using T7 and/or T7-terminal sequencing primers. Plasmids coding for Rv0045c variants were transformed into *E. coli* BL21 (DE3) RIPL cells, and variants of Rv0045c were overexpressed and purified using the same procedure as for wild-type Rv0045c. For variants of Rv0045c involving tyrosine and tryptophan substitutions, the extinction coefficients were adjusted to correct for the gain/loss of a chromophore (Rv0045c+Tyr ε^{280} = 37 470 M^{-1} cm^{-1} ; Rv0045c+Trp ε^{280} = 41 480 M^{-1} cm^{-1}).[19]

Thermal Stability Measurement. The thermal stability of Rv0045c and Rv0045c variants was determined using differential scanning fluorimetry.[20,21] Rv0045c protein (0.30 mg/mL) was diluted in triplicate in PBS containing a 1:250 dilution of 5000× Sypro Orange dye (Invitrogen, Carlsbad, CA). The samples were heated from 15 to 80 °C at 1.0 °C/min in a thermocycler (Biorad C1000 Thermocycler with CFX96 Real-time System, Hercules, CA), and the change in Sypro Orange fluorescence was followed over time (λ_{ex} = 450–490 nm, λ_{em} = 610–650 nm). The midpoint denaturation temperature (T_m) was determined by plotting the first derivative of fluorescence versus temperature and finding the temperature at the midpoint of the transition.

Kinetic Measurements with Fluorogenic Hydrolase Substrates. The enzymatic activity of Rv0045c and variants of Rv0045c was measured using fluorogenic hydrolase substrates (Figure 1A,B) in a 96-well microplate assay.[18,22,23] Fluorogenic substrates were synthesized as previously described.[18,22,24] Fluorogenic substrates were prepared as stock solutions in DMSO (10 mM) and were diluted into PBS containing acetylated BSA (Sigma; 0.1 mg/mL) to starting concentrations between 100 and 1000 μM, depending on the K_m value of Rv0045c for the substrate. The majority of the substrates (substrates **1**–**18**) had the same starting concentration (100 μM) with fluorine containing substrates **19**–**21** requiring higher starting concentrations (1000 μM). Eight serial dilutions (1:2; 60 μL into 180 μL total volume) of each substrate were made using PBS–BSA. Fluorogenic substrate dilutions (95 μL) were then transferred to a black 96-well microplate (Corning, Lowell, MA). Enzyme-catalyzed hydrolysis was initiated by addition of Rv0045c or variants of Rv0045c (5 μL of 150 μg/mL; final concentration Rv045c = 7.5 μg/mL) to diluted fluorogenic substrates in the black 96-well microplate (100 μL final volume), and the fluorescence change (λ_{ex} = 485 nm, λ_{em} = 528 nm) was measured for 4 min at 25 °C on a Biotek Synergy H1 multimode plate reader (Biotek Instruments; Winooski, VT). The fluorescence change was converted to molar concentrations using a fluorescein standard curve (300 nM–2.3 nM for higher starting concentrations), whose fluorescence was measured simultaneously. The initial rates of the enzyme-catalyzed reactions were measured in triplicate and plotted versus fluorogenic substrate concentration. The saturation enzyme kinetic traces were fitted to a standard Michaelis–Menten equation using Origin 6.1 software (OriginLab Corp., Northhampton, MA), and values for k_{cat}, K_M, and k_{cat}/K_M were calculated. The error of the hyperbolic line fit was extrapolated to the tabulated values for the kinetic constants.

Loop Modeling. The flexible loop in Rv0045c (residues 194–204; sequence QRGTVALMHGE) was modeled using the FALC online loop-modeling server.[25] The five best loop models based on DFIRE scores were determined using the FALCm method, which combines fragment assembly, analytical loop closure, and local gradient minimization.[25,26]

RESULTS

Substrate Specificity of Rv0045c. On the basis of computer modeling and limited kinetic analysis, Rv0045c was predicted to prefer short, linear substrates of less than six carbons.[13] To define its precise substrate specificity and potential biological substrates, the kinetic activity of Rv0045c was characterized against a library of fluorogenic hydrolase substrates with a diversity of acyl ester substituents (Figure 1A,B). This library of acyloxymethyl ether substrates features broad substrate diversity, representative substrate building blocks for multiple hydrolase classes, low background fluorescence, high kinetic sensitivity, and reproducible reactivity.[18,22,24] Kinetic data for Rv0045c against 18 of the 21 different fluorogenic substrates showed classic hyperbolic saturation enzyme kinetics and were fitted to the Michaelis–Menten equation to determine values for k_{cat}, K_m, and k_{cat}/K_m (Supplemental Table 1, Supporting Information). Three aromatic substrates (**15**, **20**, **21**) failed to produce saturation kinetic curves even at higher substrate concentrations.

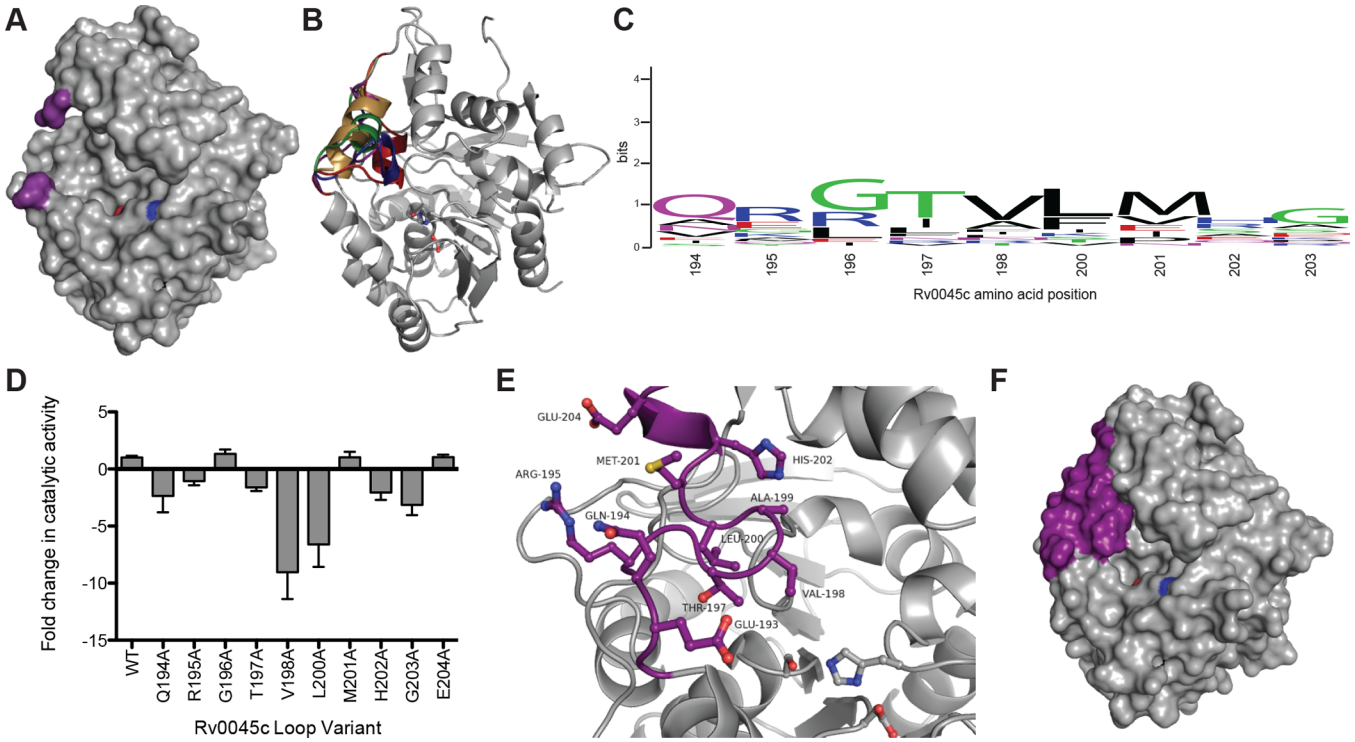

Figure 2. Modeling of the flexible loop covering the binding pocket in Rv0045c. (A) Basic three-dimensional surface structure of Rv0045c. The residues connecting the flexible loop that was missing from original structure of Rv0045c (PDB: 3P2M) are highlighted in purple. The catalytic serine is shown in red and the catalytic histidine is in blue. (B) Top ranked loop models based on FALC model of the flexible loop in Rv0045c. The top five loop models from FALCm based on fragment assembly, analytical loop closure, and gradient minimization are colored separately.[25] The DFIRE energy for all five models was within 5.[26] (C) Conservation of flexible loop residues across bacterial homologues of Rv0045c. Sequences aligned using ClustalW and relative weightings performed using Weblogo.[40,41] Detailed sequence analysis along with percent identity between homologues given in Supplemental Table 3, Supporting Information. (D) Relative catalytic activity of Rv0045c loop variants. The catalytic activity of each of the Rv0045c variants was determined against substrates **6** and normalized based on the activity of wild-type Rv0045c against each substrate. Variants with lower activity than the wild-type enzyme were given negative ratios. Detailed kinetic and thermal stability analysis for flexible loop variants are given in Supplemental Table 3. (E, F) Final loop model for Rv0045c. The final model was chosen based on a combination of alanine scanning mutagenesis results (D) and computational modeling (B). The loop model is shown in sticks (E) with the individual residues labeled to highlight the proximity of Val198 and Leu200 to the active site and in surface representation (F) to illustrate the importance of the loop to defining the binding pocket of Rv0045c.

On the basis of the comparison of k_{cat}/K_m values (Figure 1C), Rv0045c strongly prefers short, straight chain acyl ester substituents with highest activity against straight chain esters with ether linkages included in the chain (substrates **6**–**8**). This preference for substrates **6**–**8** with highest activity against substrate **6** matches the substrate specificity pattern of the ybfF hydrolase.[18] Rv0045c also showed bell-shaped substrate reactivity against linear alkyl substrates with maximal activity against a butyl ester and steep decreases in activity with even single carbon additions to the alkyl chain (Figure 1D). Besides linear ester substrates, Rv0045c had measurable activity (k_{cat}/K_m > 10 M^{-1} s^{-1}) against small, unsaturated esters (**9**, **10**), nonaromatic cyloalkyl esters (**11**–**13**), and a fluorinated propyl ester (**19**), but strongly selects against reactivity with aromatic and tertiary esters (Figure 1C). Although Rv0045c has been modeled to fit a five-carbon ester in its binding pocket, how Rv0045c strongly selects for these short alkyl substrates was unclear, as a key substrate-binding loop was not present in the crystal structure of Rv0045c.

Modeling and Kinetic Analysis of Flexible Loop. To clarify the binding pocket structure of Rv0045c, the amino acid residues encoding the missing flexible loop were modeled onto Rv0045c. The loop model was constructed using the validated modeling program FALC (fragment assembly and analytical loop closure), an *ab initio* loop modeling method specifically optimized for refining flexible loops with ill-defined electron density from crystal structures.[25] Using FALC, a series of potential conformations for this Rv0045c loop were modeled with the top five lowest energy conformations shown in Figure 2B.[25] As these loop residues showed little sequence conservation across bacterial homologues (Figure 2C), alanine-scanning mutagenesis was performed on the loop residues (residues 194–204) to assign their importance to the catalytic activity of Rv0045c and to select the best loop model.

To perform alanine-scanning mutagenesis, each of the loop residues was individually substituted with alanine, and the resulting Rv0045c variant was purified to homogeneity and characterized for relative thermal stability and catalytic activity against the best fluorogenic substrate (**6**) (Supplemental Table 2, Supporting Information). For relative thermal stabilities, all of the loop variants had T_m values within 1 °C of wild-type Rv0045c, reaffirming the flexibility and lack of structural contributions of this loop (Supplemental Table 2).[13] In comparison, loop variants had significant variations (>10-fold) in catalytic activity from wild-type Rv0045c (Figure 2D). This significant change in catalytic activity without affecting the stability of Rv0045c indicates that these loop residues are directly involved in substrate binding or orientation within the

dx.doi.org/10.1021/bi501108u | *Biochemistry* 2014, 53, 7386–7395

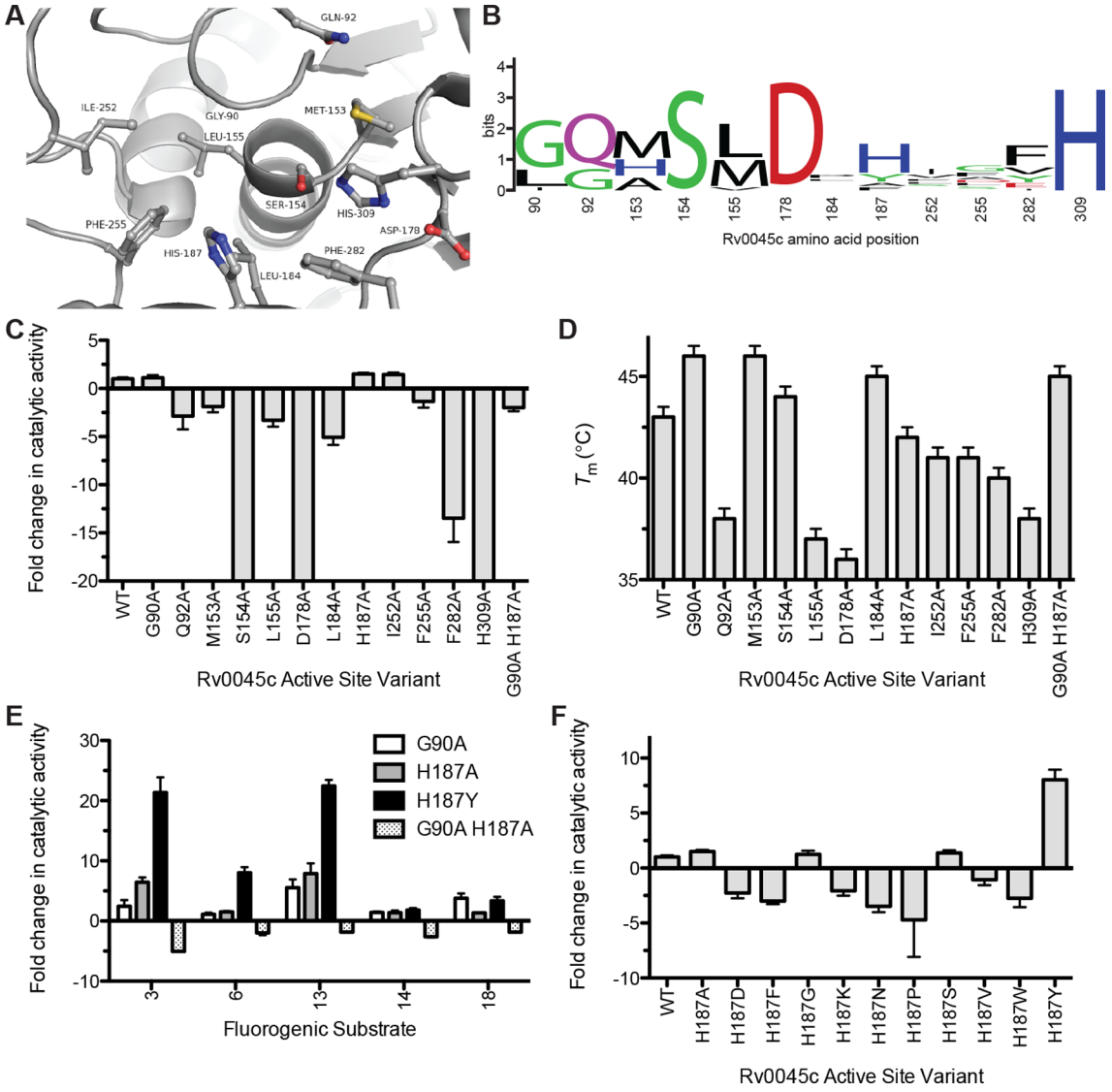

Figure 3. Importance of the binding pocket and active site amino acids to the catalytic activity and thermal stability of Rv0045c. (A) Binding pocket and catalytic residues substituted with alanine in Rv0045c. Each of the residues shown in ball and stick was individually substituted with alanine and the relative contribution of each side-chain to the catalytic activity and thermal stability determined. (B) Conservation of binding pocket residues across bacterial homologues of Rv0045c. Sequences aligned using ClustalW and relative weightings performed using Weblogo.[40,41] Detailed sequence analysis along with percent identity between homologues given in Supplemental Table 3. (C) Relative catalytic activity of Rv0045c binding pocket variants. The catalytic activity of each of the Rv0045c variants was determined against substrates **6** and normalized based on the activity of wild-type Rv0045c against each substrate. Variants with lower activity than the wild-type enzyme were given negative ratios. Detailed kinetic and thermal stability analysis for binding pocket variants are given in Supplemental Table 4. (D) Thermal stability of Rv0045c variants. The thermal stability of each variant was determined by measuring the increase in Sypro Orange fluorescence in response to increasing temperature. Results are shown with their standard error values. (E) Substrate specificity of G90A, H187A, H187Y, and G90A H187A variants of Rv0045c. Experiments were conducted and are shown the same as (C), except using the fluorogenic substrate specified (number from Figure 1B). (F) Relative catalytic activity of H187X variants of Rv0045c. Experiments were conducted and are shown the same as (C). Detailed kinetic and thermal stability analysis for H187X variants are given in Supplemental Table 6.

Rv0045c active site. Key residues (Val198 and Leu200) to the catalytic activity were congregated toward the center of the loop and flanked by residues with no observed role in the catalytic activity (Figure 2D). On the basis of the relative importance of loop residues to the catalytic activity of Rv0045c, one loop model was chosen that best matched the computational and alanine scanning data (Figure 2E). The orientation of this loop model places key catalytic residues (Val198 and Leu200) in closest proximity to the active site and available for direct interaction with incoming substrates. This loop orientation also positions residues not involved in the catalytic activity (Arg195, Glu196, Met201, and Glu204) away from the active site. The location of the chosen loop model for Rv0045c also recapitulates the enclosed substrate-binding pocket of ybfF and creates a binding pocket with the appropriate size to accommodate the preferred four atom substrates (Figure 2F).[14]

Analysis of Binding Pocket and Active Site of Rv0045c. With the structure of the flexible, connecting loop inserted into the structure of Rv0045c (Figures 2E,F), the binding pocket shape and orientation shifts from the small, shallow binding pocket originally modeled to bind *p*-nitrophenyl caprylate to a larger, binding cavity similar to ybfF

dx.doi.org/10.1021/bi501108u | *Biochemistry* 2014, 53, 7386−7395

hydrolases with space to accommodate a range of acyl ester substrates.[13] To build a complete model of the binding pocket of Rv0045, a comprehensive alanine scan of the binding pocket and active site of Rv0045c was constructed using 12 additional alanine variants of Rv0045c (Figure 3A). As compared to the flexible loop residues, the active site and binding pocket residues showed much wider degrees of sequence conservation across bacterial homologues (Figure 3B), varying from the absolutely conserved catalytic triad residues (Ser154, Asp178, and His309) to only slightly conserved binding pocket residues (Ile252 and Phe255). Each of the 12 residues was individually substituted with alanine; the resulting protein was then purified to homogeneity (Supplemental Figure 2) and characterized for enzymatic activity and thermal stability (Supplemental Table 3).

Overall, the relative catalytic activity (as measured by k_{cat}/K_M) differences between Rv0045c variants and wild-type Rv0045c ranged from significant decreases in catalytic activity (>100-fold for the catalytic triad) to slight increases in catalytic activity (<5-fold increase for G90A, H187A, I252A) (Figure 3C). Deletion of each of the catalytic triad residues individually destroyed the catalytic activity of Rv0045c with the most significant decrease observed for the essential nucleophilic serine residue (Ser154). Outside the catalytic triad, the nine other binding pocket residues played smaller roles than even the flexible loop residues in determining the catalytic activity of Rv0045c (Figure 3C). The only variant with a significant change in catalytic activity (>10-fold) was F282A. Phe282 is located adjacent to the catalytic serine and is likely necessary to maintain proper positioning of the serine nucleophile (Figure 3A). The majority of the remaining binding pocket residues showed only minimal importance to the catalytic activity of Rv0045c even with fairly substantial changes in the thermal stability of Rv0045c variants (Figure 3D).

Even though the majority of the binding pocket residues showed only minor roles in the catalytic activity, three residues (G90A, H187A, I252A) showed slight but significant increases in their relative catalytic activity compared to wild-type Rv0045c (Figure 3C,D). Two of these residues (Gly90 and His187) are positioned at the entrance to the binding pocket of Rv0045c and Ile252 packs against Gly90 in the back of the binding pocket cavity (Figure 3A). The relative positioning of Gly90 and His187 on opposing sides of the entrance to the binding pocket suggested a potential role in maintaining the narrow substrate specificity of Rv0045c. To measure the relative importance of these positions to the substrate specificity of Rv0045c, the catalytic activity of the G90A and H187A Rv0045c variants was measured against a range of structurally distinct fluorogenic substrates (substrates **3**, **6**, **13**, **14**, **18**; Figure 3E; Supplemental Table 4). Against a straight chain alkyl substrate (**3**) and a small cycloalkyl substrate (**13**), substitution of G90A and H187A significantly increased the catalytic activity of Rv0045c (3−8 fold) with larger increases observed for H187A (Figure 3E). This effect was diminished with a larger cycloalkyl (**14**) and a tertiary ester substrate (**18**), but activities higher than wild-type Rv0045c were still measured with all five substrates. To see if this catalytic effect was synergistic, a double variant G90A/H187A Rv0045c was constructed, and its catalytic activity was measured against the subset of fluorogenic substrates (Figure 3E). The double variant had nearly identical thermal stability to the wild-type protein and individual single variants (Figure 3D), suggesting that the overall folded stability of this variant is not significantly changed. The G90A/H187A variant however showed reduced catalytic activity toward all five different fluorogenic substrates (Figure 3E). Thus, independent substitution of Gly90 and His187 broadens the substrate specificity and increases the catalytic activity of Rv0045c, but the substitutional effect was not additive.

The comprehensive alanine-scanning mutagenesis of the flexible loop and binding pocket of Rv0045c provided a global picture of the residues controlling the substrate specificity and catalytic activity of Rv0045c (Figures 4A,B). Outside the essential catalytic triad residues (red), only a few residues distributed on both sides of the binding pocket contribute significantly to the catalytic activity of Rv0045c (orange). In this global picture, loop residues distributed over the binding pocket serve as essential a role in substrate recognition and catalysis as binding pocket residues surrounding the active site (Figures 2D and 3C). Instead of the majority of substitutions significantly decreasing the catalytic activity of Rv0045c, Rv0045c was surprisingly easily modulated to have increased activity toward a diverse set of substrates with independent substitution of Gly90 and His187. This modulation was easily accomplished with only single amino acid substitutions to these selectivity residues that flank the binding pocket (green).

Substrate Selectivity Residue Controls the Activity of Rv0045c. Among the two selectivity residues, the relative positioning and sequence conservation of His187 was especially intriguing, as the analogous position in the ybfF hydrolase is completely conserved as a tyrosine residue.[14] This tyrosine also makes two direct hydrogen bonds to the malonate substrate bound in the crystal structure of ybfF from *E. coli*, suggesting a central role for this tyrosine in substrate recognition (Figure 4C).[14] To determine the role of His187 in controlling the substrate specificity of Rv0045c, His187 was substituted with 10 amino acids from across different structural and chemical classes and the relative thermal stability and catalytic activity of the variants characterized (Supplemental Table 5, Supporting Information).

Similar to the H187A variant, the majority of the substitutions at position 187 made only minor changes to the thermal stability of Rv0045c even with large changes to the amino acid structure, including substitutions with cyclic (proline), negatively charged (aspartate), and large hydrophobic (tryptophan) residues (Supplemental Table 5). The catalytic activity of the different His187 substitutions, however, varies widely with the majority of the substitutions leading to small (<5-fold) decreases in the catalytic activity (Figure 3F). Similar to the alanine substitution (H187A), exchange of position 187 with other small amino acids (glycine and serine) led to small but significant increases in the relative catalytic activity. The largest shift in the catalytic activity was observed with the analogous substitution to ybfF hydrolases (H187Y; Figure 3F). H187Y Rv0045c had an 8-fold increase in the relative k_{cat}/K_m values for substrate **6** compared to wild-type Rv0045c. Similar to the G90A and H187A variants, the increased activity of the H187Y variant was maintained across different fluorogenic substrates and showed significantly higher increases in activity (>20-fold) with substrates **3** and **13** (Figure 3E). Additionally, like G90A and H187A, the increased activity of H187Y was diminished with larger or sterically constrained substrates (**14** and **18**). This position (His187) in Rv0045c thus serves as a central substrate selectivity residue, as many substitutions decreased the activity, small substitutions slightly increased the activity, and tyrosine substitution drastically

dx.doi.org/10.1021/bi501108u | *Biochemistry* 2014, 53, 7386−7395

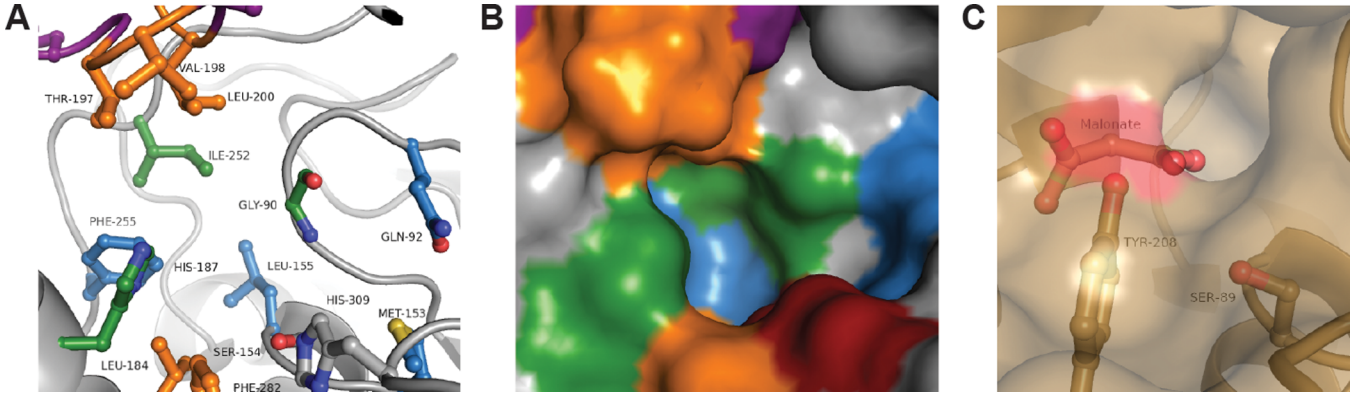

Figure 4. Binding pocket structures of Rv0045c and ybfF hydrolases. (A and B) Relative contributions of binding pocket and loop residues to the catalytic activity of Rv0045c. Stick (A) and surface representations (B) of the binding pocket of Rv0045c colored coded for their relative contributions to the catalytic activity of Rv0045c against substrate **6**. Colors represent relative changes to the catalytic activity (k_{cat}/K_M) upon substitution to alanine: red (>30-fold decrease); orange (>5-fold decrease); blue (<5-fold decrease) for binding pocket; purple (<5-fold decrease) for loop; green (>1-fold increase). (C) Binding pocket of the ybfF hydrolase from *E. coli* (PDB: 3BF8). The tyrosine residue (Tyr208) in ybfF that is a structural homologue to His187 in Rv0045c is shown hydrogen bonded to the cocrystallized malonate. The catalytic serine residue (Ser89) is shown in sticks for context.

increased the catalytic activity and broadened the substrate specificity of Rv0045c.

DISCUSSION

Hydrolases control essential roles in the metabolic and virulence pathways of *M. tuberculosis* and other mycobacteria.[5,27] Among mycobacterial hydrolases, the Rv0045c hydrolase from *M. tuberculosis* is distinct from the normal Lip and Cut family hydrolases in *M. tuberculosis*, whose relative substrate specificity and biological importance have been characterized using a variety of methodologies.[6,8,28] Rv0045c represents a unique bacterial subfamily of proposed metabolic hydrolases, along with the structurally similar ybfF hydrolases from Gram-negative bacteria like *E. coli* and *Vibrio cholerae* and *E*-2AMS enzymes in *M. loti*.[13,14,18] The strong selectivity for four atom ether alkyl substrates in both Rv0045c and ybfF enzymes indicates similar biological substrates for these structurally conserved bacterial hydrolases. On the basis of cocrystallization and kinetic analysis, ybfF was proposed to recognize and hydrolyze malonyl- or succinyl-CoA thioesters.[14] The binding pocket of Rv0045c was, however, modeled to only contain sufficient space for a five-carbon linear acyl ester substituent, but refinement of the binding pocket model was hindered by the lack of electron density for the flexible loop overhanging the active site and connecting the cap and α/β hydrolase domains (Figure 2A).[13] Computational insertion of the loop to Rv0045c and loop refinement by alanine scanning mutagenesis provided a complete picture of the binding pocket of Rv0045c (Figure 2). In the completed binding pocket of Rv0045c, the flexible loop creates an enclosed cavity and recapitulates the binding pocket of the ybfF hydrolase.[14] Although Rv0045c does not have two distinct bifurcated lobes to its binding pocket like ybfF, the positioning and proposed flexibility of the connecting loop on Rv0045c could rearrange to enclose bound substrates and increase substrate selectivity, providing Rv0045c with a substrate selectivity mechanism similar to other lipases and hydrolases.[29−31]

In addition to the flexible loop, two residues bracketing the entrance to this enclosed binding pocket also control the substrate selectivity of Rv0045c. These selectivity residues (Gly90 and His187) together control the substrate access channel of Rv0045c and when mutated reduce the substrate selectivity of Rv0045c (Figure 3). The increased catalytic activity and broadened substrate specificity of the Gly90 and His187 variants is not solely due to removal of steric occlusion of the binding pocket, as insertion of the larger alanine residue for Gly90 and the larger tyrosine residue for His187 would likely increase the steric hindrance in the binding pocket. Instead, the potential combined effect of the opposing positive charge on His187 and the partial negative charge on the carbonyl oxygen of Gly90 may create a stereoelectronic selectivity filter for the Rv0045c binding pocket. The presence of similar polar residues and stereoelectronic filters in close proximity to the active site has been identified as a key predictor of the broadened reactivity and substrate specificity of promiscuous enzymes.[32] The reduced kinetic activity of the G90A H187A Rv0045c variant, however, indicates that Gly90 and His187 function independently to provide redundant control over the substrate selectivity of Rv0045c. A full understanding of the effect of these mutations on substrate binding will however require future crystallographic analysis, as even single alanine substitutions can significantly shift the substrate-binding mode in a hydrolase.[33,34]

The role of His187 in controlling the substrate specificity of Rv0045c is especially intriguing, as the catalytic activity of Rv0045c was increased by 8−20-fold with the H187Y substitution, depending on the acyl ester substrate (Figure 3E). The mechanism for this shift in substrate specificity with tyrosine substitution can be inferred based on changes in the catalytic activity with different amino acid substitutions. For instance, the increased activity of H187Y across multiple fluorogenic substrates shows that the increased activity is not due to a specific hydrogen bonding interaction between the phenolic alcohol of tyrosine and the ether oxygen of substrate **6** (Figures 4A−C). The decreased catalytic activity for the H187F and H187W variants also indicates that the increased catalytic activity of H187Y Rv0045c is not merely due to hydrophobic stacking with the fluorescein core of the fluorogenic substrate or even reorientation of the binding pocket. The importance of the alcohol portion of the ester bond to the catalytic activity of Rv0045c was not investigated in this study but may play a connected role in controlling the substrate selectivity of

dx.doi.org/10.1021/bi501108u | *Biochemistry* 2014, 53, 7386−7395

Rv0045c. For the catalytic activity against various acyl ester substituents (Figure 1B), the comparison of the H187Y and H187F variants instead argues that the additional phenolic alcohol on the tyrosine substitution plays a new role in substrate stabilization or catalytic reactivity. The large shift in the catalytic activity of Rv0045c with this single substitution at the entrance to the binding pocket (Figures 4A,B) also identifies this conserved structural position in the Rv0045c hydrolase as a key residue controlling its substrate selectivity. The difference in the amino acid residue at position 187 between Rv0045c and ybfF and the concomitant change in catalytic activity upon residue swapping suggests that Rv0045c and ybfF likely recognize different biological substrates. Thus, while ybfF catalyzes the hydrolysis of thioester bonds in malonyl- and/or succinyl-CoA, Rv0045c maintains similar substrate specificity but uses the histidine at position 187 to recognize a slightly different and yet unidentified biological substrate.[14] The sequence space for these two hydrolases may however be amenable to recombinatorial engineering where shuffling of limited residues between homologous enzymes can significantly broaden the chemical reactivity and substrate specificity of homologous enzymes.[35] The presence of this broad substrate specificity and easy adaptability in these families of hydrolases matches with the observed higher promiscuity present in lipid metabolizing enzymes and in enzymes from actinobacteria.[36]

Members of the ybfF hydrolase family have also drawn interest due to their biocatalytic potential.[16−18] For example, the ybfF hydrolase from *E. coli* utilizes its bifurcated binding pocket to efficiently catalyze a rapid, stereoselective reaction with 1,2-*O*-isopropyideneglycerol (IPG) esters, a potential pharmaceutical starting material in the production of *β*-blockers, prostaglandins, and leukotrienes.[16,17] An unusual feature to the bioengineering of ybfF was the decoupling between the roles of individual binding pocket residues in maintaining the folded stability and catalytic activity of ybfF.[18] Similar decoupling was also observed in Rv0045c, as changes in the catalytic activity did not correlate with changes in thermal stability. For example, substitution of Q92A and L155A caused 5−6 °C changes in the T_m values but only led to minor changes in the relative k_{cat}/K_m values (<5-fold) from wild-type Rv0045c (Figure 3; Supplemental Table 4, Supporting Information). This conserved pattern of decoupled roles of binding pocket residues in maintaining the thermal stability and catalytic activity suggests evolutionary selection for this relative independence in this protein family.[37] Additionally, the conserved structural α/β hydrolase fold for Rv0045c and ybfF appears to have great structural plasticity, making their structural arrangement an excellent scaffold for ongoing protein engineering.[18] Whether this structural plasticity carries over into the structurally similar *E*-2AMS hydrolases is an interesting area for future investigation, especially as *E*-2AMS hydrolases already catalyze an unusual chemical conversion.[15]

CONCLUSIONS

Rv0045c is a unique α/β hydrolase family enzyme from *M. tuberculosis*. Comparison of the substrate specificity of Rv0045c and other bacterial hydrolases places Rv0045c into the family of small, metabolic hydrolases. Rv0045c has a broad, open binding pocket but shows narrow substrate specificity for short, straight chain alkyl substrates. Substrate selectivity residues bracketing the binding pocket regulate this narrow substrate specificity and differentiate its substrate specificity from structurally homologous hydrolases. The easy manipulation of the substrate selectivity of Rv0045c make it an interesting enzyme engineering target where the key substrate selectivity residues identified in this study could be used as starting points for future saturation mutagenesis studies.[38] With its unique structural features, lack of sequence and structural conservation in mammals, and potential role in metabolism, Rv0045c also represents an interesting hub in mycobacterial metabolism, where the current structural analysis could be used to develop chemical modulators of Rv0045c activity to study its biological activity and its importance under different growth conditions.

ASSOCIATED CONTENT

Supporting Information

Detailed kinetic data for Rv0045c and its variants, example kinetic traces, sequence alignment for binding pocket residues in Rv0045c, PCR primers used for mutagenesis, gel analysis of Rv0045c and its variants, and PDB coordinates for the loop structure of Rv0045c. This material is available free of charge via the Internet at http://pubs.acs.org.

AUTHOR INFORMATION

Corresponding Author

*Phone: 317-940-9062. E-mail: rjjohns1@butler.edu.

Author Contributions

§J.K.L and C.P.S. contributed equally to this work.

Funding

R.J.J., G.C.H., J.K.L, and C.P.S. were supported by a grant from the National Science Foundation (DUE-1140526). C.T.A. and L.D.L. were supported by the Howard Hughes Medical Institute.

Notes

The authors declare no competing financial interest.

ACKNOWLEDGMENTS

We are grateful to Dr. Hai Pang (Tsinghua University) who kindly provided the expression plasmid for Rv0045c. We thank CH463 students from Spring 2012 and 2013 for assistance with preliminary enzyme purification and enzymatic analysis.

ABBREVIATIONS:

DSF, differential scanning fluorimetry; *E*- 2AMS, (*E*)-2-(acetamidomethylene) succinate; FALC, fragment assembly and analytical loop closure; IPG, 1,2-*O*-isopropyideneglycerol; LB, Luria−Bertani broth; MDR, multi drug resistant TB; MWCO, molecular weight cutoff; Ni-NTA, nickel-nitrilotriacetic acid; PDB, protein data bank; Rv0045c, serine hydrolase from *Mycobacterium tuberculosis*; TAG, triacylglycerol; TB, tuberculosis; XDR, extensive drug resistant TB

REFERENCES

(1) Peyron, P., Vaubourgeix, J., Poquet, Y., Levillain, F., Botanch, C., Bardou, F., Daffe, M., Emile, J. F., Marchou, B., Cardona, P. J., de Chastellier, C., and Altare, F. (2008) Foamy macrophages from tuberculous patients' granulomas constitute a nutrient-rich reservoir for *M. tuberculosis* persistence. *PLoS Pathog. 4*, e1000204.

(2) Daniel, J., Maamar, H., Deb, C., Sirakova, T. D., and Kolattukudy, P. E. (2011) Mycobacterium tuberculosis uses host triacylglycerol to accumulate lipid droplets and acquires a dormancy-like phenotype in lipid-loaded macrophages. *PLoS Pathog. 7*, e1002093.

(3) Garton, N. J., Christensen, H., Minnikin, D. E., Adegbola, R. A., and Barer, M. R. (2002) Intracellular lipophilic inclusions of mycobacteria in vitro and in sputum. *Microbiology 148*, 2951−2958.

(4) Cole, S. T., Brosch, R., Parkhill, J., Garnier, T., Churcher, C., Harris, D., Gordon, S. V., Eiglmeier, K., Gas, S., Barry, C. E., 3rd, Tekaia, F., Badcock, K., Basham, D., Brown, D., Chillingworth, T., Connor, R., Davies, R., Devlin, K., Feltwell, T., Gentles, S., Hamlin, N., Holroyd, S., Hornsby, T., Jagels, K., Krogh, A., McLean, J., Moule, S., Murphy, L., Oliver, K., Osborne, J., Quail, M. A., Rajandream, M. A., Rogers, J., Rutter, S., Seeger, K., Skelton, J., Squares, R., Squares, S., Sulston, J. E., Taylor, K., Whitehead, S., and Barrell, B. G. (1998) Deciphering the biology of *Mycobacterium tuberculosis* from the complete genome sequence. *Nature 393*, 537−544.

(5) Singh, G., Jadeja, D., and Kaur, J. (2010) Lipid hydrolizing enzymes in virulence: *Mycobacterium tuberculosis* as a model system. *Crit. Rev. Microbiol. 36*, 259−269.

(6) Delorme, V., Diomande, S. V., Dedieu, L., Cavalier, J. F., Carriere, F., Kremer, L., Leclaire, J., Fotiadu, F., and Canaan, S. (2012) MmPPOX inhibits *Mycobacterium tuberculosis* lipolytic enzymes belonging to the hormone-sensitive lipase family and alters mycobacterial growth. *PLoS One 7*, e46493.

(7) West, N. P., Cergol, K. M., Xue, M., Randall, E. J., Britton, W. J., and Payne, R. J. (2011) Inhibitors of an essential mycobacterial cell wall lipase (Rv3802c) as tuberculosis drug leads. *Chem. Commun. (Cambridge) 47*, 5166−5168.

(8) West, N. P., Chow, F. M. E., Randall, E. J., Wu, J., Chen, J., Ribeiro, J. M. C., and Britton, W. J. (2009) Cutinase-like proteins of *Mycobacterium tuberculosis*: characterization of their variable enzymatic functions and active site identification. *FASEB J. 23*, 1694−1704.

(9) Kourist, R., Jochens, H., Bartsch, S., Kuipers, R., Padhi, S. K., Gall, M., Bottcher, D., Joosten, H. J., and Bornscheuer, U. T. (2010) The alpha/beta-hydrolase fold 3DM database (ABHDB) as a tool for protein engineering. *ChemBioChem 11*, 1635−1643.

(10) Jochens, H., Hesseler, M., Stiba, K., Padhi, S. K., Kazlauskas, R. J., and Bornscheuer, U. T. (2011) Protein engineering of alpha/beta-hydrolase fold enzymes. *ChemBioChem 12*, 1508−1517.

(11) Xu, L., Guo, J., Zheng, X., Wen, T., Sun, F., Liu, S., and Pang, H. (2010) Crystallization and preliminary X-ray analysis of a novel esterase Rv0045c from *Mycobacterium tuberculosis*. *Acta Crystallogr., Sect. F 66*, 1579−1582.

(12) Guo, J., Zheng, X., Xu, L., Liu, Z., Xu, K., Li, S., Wen, T., Liu, S., and Pang, H. (2010) Characterization of a novel esterase Rv0045c from *Mycobacterium tuberculosis*. *PLoS One 5*, e13143.

(13) Zheng, X., Guo, J., Xu, L., Li, H., Zhang, D., Zhang, K., Sun, F., Wen, T., Liu, S., and Pang, H. (2011) Crystal structure of a novel esterase Rv0045c from *Mycobacterium tuberculosis*. *PLoS One 6*, e20506.

(14) Park, S. Y., Lee, S. H., Lee, J., Nishi, K., Kim, Y. S., Jung, C. H., and Kim, J. S. (2008) High-resolution structure of ybfF from *Escherichia coli* K12: a unique substrate-binding crevice generated by domain arrangement. *J. Mol. Biol. 376*, 1426−1437.

(15) McCulloch, K. M., Mukherjee, T., Begley, T. P., and Ealick, S. E. (2010) Structure determination and characterization of the vitamin B6 degradative enzyme (*E*)-2-(acetamidomethylene)succinate hydrolase. *Biochemistry 49*, 1226−1235.

(16) Godinho, L. F., Reis, C. R., Tepper, P. G., Poelarends, G. J., and Quax, W. J. (2011) Discovery of an *Escherichia coli* esterase with high activity and enantioselectivity toward 1,2-*O*-isopropylideneglycerol esters. *Appl. Environ. Microbiol. 77*, 6094−6099.

(17) Godinho, L. F., Reis, C. R., van Merkerk, R., Poelarends, G. J., and Quax, W. J. (2012) An esterase with superior activity and enantioselectivity towards 1,2-O-Isopropylideneglycerol esters obtained by protein design. *Adv. Synth. Catal. 354*, 3009−3015.

(18) Ellis, E. E., Adkins, C. T., Galovska, N. M., Lavis, L. D., and Johnson, R. J. (2013) Decoupled roles for the atypical, bifurcated binding pocket of the ybfF hydrolase. *ChemBioChem 14*, 1134−1144.

(19) Gasteiger, E., Hoogland, C., Gattiker, A., Wilkins, M. R., Appel, R. D., and Bairoch, A. (2005) Protein identification and analysis tools on the ExPASy server, In *The Proteomics Protocols Handbook*, pp 571−607, Springer, Berlin.

(20) Niesen, F. H., Berglund, H., and Vedadi, M. (2007) The use of differential scanning fluorimetry to detect ligand interactions that promote protein stability. *Nat. Protoc. 2*, 2212−2221.

(21) Simeonov, A. (2013) Recent developments in the use of differential scanning fluorometry in protein and small molecule discovery and characterization. *Expert Opin. Drug Discovery 8*, 1071−1082.

(22) Hedge, M. K., Gehring, A. M., Adkins, C. T., Weston, L. A., Lavis, L. D., and Johnson, R. J. (2012) The structural basis for the narrow substrate specificity of an acetyl esterase from *Thermotoga maritima*. *Biochim. Biophys. Acta 1824*, 1024−1030.

(23) Filippova, E. V., Weston, L. A., Kuhn, M. L., Geissler, B., Gehring, A. M., Armoush, N., Adkins, C. T., Minasov, G., Dubrovska, I., Shuvalova, L., Winsor, J. R., Lavis, L. D., Satchell, K. J., Becker, D. P., Anderson, W. F., and Johnson, R. J. (2013) Large scale structural rearrangement of a serine hydrolase from *Francisella tularensis* facilitates catalysis. *J. Biol. Chem. 288*, 10522−10535.

(24) Lavis, L. D., Chao, T.-Y., and Raines, R. T. (2011) Synthesis and utility of fluorogenic acetoxymethyl ethers. *Chem. Sci. 2*, 521−530.

(25) Ko, J., Lee, D., Park, H., Coutsias, E. A., Lee, J., and Seok, C. (2011) The FALC-Loop web server for protein loop modeling. *Nucleic Acids Res. 39*, W210−214.

(26) Yang, Y., and Zhou, Y. (2008) Ab initio folding of terminal segments with secondary structures reveals the fine difference between two closely related all-atom statistical energy functions. *Protein Sci. 17*, 1212−1219.

(27) Dedieu, L., Serveau-Avesque, C., Kremer, L., and Canaan, S. (2013) Mycobacterial lipolytic enzymes: a gold mine for tuberculosis research. *Biochimie 95*, 66−73.

(28) Deb, C., Daniel, J., Sirakova, T. D., Abomoelak, B., Dubey, V. S., and Kolattukudy, P. E. (2006) A novel lipase belonging to the hormone-sensitive lipase family induced under starvation to utilize stored triacylglycerol in *Mycobacterium tuberculosis*. *J. Biol. Chem. 281*, 3866−3875.

(29) van Tilbeurgh, H., Egloff, M. P., Martinez, C., Rugani, N., Verger, R., and Cambillau, C. (1993) Interfacial activation of the lipase-procolipase complex by mixed micelles revealed by X-ray crystallography. *Nature 362*, 814−820.

(30) Rehm, S., Trodler, P., and Pleiss, J. (2010) Solvent-induced lid opening in lipases: a molecular dynamics study. *Protein Sci. 19*, 2122−2130.

(31) Saravanan, P., Dubey, V. K., and Patra, S. (2012) Potential selective inhibitors against Rv0183 of *Mycobacterium tuberculosis* targeting host lipid metabolism. *Chem. Biol. Drug Des. 79*, 1056−1062.

(32) Chakraborty, S., and Rao, B. J. (2012) A measure of the promiscuity of proteins and characteristics of residues in the vicinity of the catalytic site that regulate promiscuity. *PLoS One 7*, e32011.

(33) Bone, R., Silen, J. L., and Agard, D. A. (1989) Structural plasticity broadens the specificity of an engineered protease. *Nature 339*, 191−195.

(34) Bone, R., Fujishige, A., Kettner, C. A., and Agard, D. A. (1991) Structural basis for broad specificity in alpha-lytic protease mutants. *Biochemistry 30*, 10388−10398.

(35) Raillard, S., Krebber, A., Chen, Y., Ness, J. E., Bermudez, E., Trinidad, R., Fullem, R., Davis, C., Welch, M., Seffernick, J., Wackett, L. P., Stemmer, W. P., and Minshull, J. (2001) Novel enzyme activities and functional plasticity revealed by recombining highly homologous enzymes. *Chem. Biol. 8*, 891−898.

(36) Carbonell, P., Lecointre, G., and Faulon, J. L. (2011) Origins of specificity and promiscuity in metabolic networks. *J. Biol. Chem. 286*, 43994−44004.

(37) Meier, S., and Ozbek, S. (2007) A biological cosmos of parallel universes: does protein structural plasticity facilitate evolution? *BioEssays 29*, 1095−1104.

(38) Reetz, M. T., Prasad, S., Carballeira, J. D., Gumulya, Y., and Bocola, M. (2010) Iterative saturation mutagenesis accelerates laboratory evolution of enzyme stereoselectivity: rigorous comparison with traditional methods. *J. Am. Chem. Soc. 132*, 9144−9152.

(39) Tian, L., Yang, Y., Wysocki, L. M., Arnold, A. C., Hu, A., Ravichandran, B., Sternson, S. M., Looger, L. L., and Lavis, L. D. (2012) Selective esterase-ester pair for targeting small molecules with cellular specificity. *Proc. Natl. Acad. Sci. U.S.A. 109*, 4756−4761.
(40) Crooks, G. E., Hon, G., Chandonia, J. M., and Brenner, S. E. (2004) WebLogo: a sequence logo generator. *Genome Res. 14*, 1188−1190.
(41) Chenna, R., Sugawara, H., Koike, T., Lopez, R., Gibson, T. J., Higgins, D. G., and Thompson, J. D. (2003) Multiple sequence alignment with the Clustal series of programs. *Nucleic Acids Res. 31*, 3497−3500.